N-body simulations of young protostellar systems

Gerwyn H Jones

November 2016

Abstract

We present an overview of the star formation processes that lead to the formation of protostars and how the recent *Herschel* Gould Belt Survey has led to renewed areas of research that we will pursue in the future. Through a series of tests, the N-body code was shown to be working at this moment in time. We propose ways of furthering our project by expanding on our N-body code and setting up initial conditions that replicate the conditions inside filamentary structures, observing the possible outcomes from these initial conditions.

1. Introduction

N-body simulations of physical systems are a key factor to solving and understanding problems in science. They can be used to help the understanding of interactions between molecules, help visualize the Brownian motion in molecular dynamics and are widely used throughout astrophysics. Astrophysical simulations are used to help predict the effects of dark matter on astronomical bodies, and can also help to understand and formulate theoretical models of phenomena such as star formation.

1.1 Star formation

Perturbations such as shock waves from nearby supernovae and collisions between two giant molecular clouds (GMC) can lead to contractions on the clouds. If the contraction of these clouds surpasses a certain radius called the Jeans radius, gravity overcomes turbulences and thermal pressure and becomes the dominant force and produces a dynamical collapse which is uncontrollable. This is process sparks the beginning of star formation. (Appenzeller, et al., 1980)

During this collapsing phase of the molecular cloud, the original molecular cloud breaks up into smaller clouds through fragmentation. During collapse, the opacity of the clouds increases and leads to an increase in temperature. As the cloud obeys the ideal gas law, the pressure built up inside the clouds increases and the fragmentation process is halted when hydrostatic equilibrium is reached. This results in the formation of a protostar.

An envelope of gas and dust surrounds the protostar which due to gravity accretes onto the protostar which increases the mass and temperature of the protostar. The lack of an envelope leads to a pre-main-sequence star (PMS star). A PMS star is a star that has yet to start hydrogen burning through nuclear fusion. Once the protostar's opacity increases to the point that the gravitational contraction causes the temperature to increase to a point that hydrogen burning can start, the star is then said to be a main-sequence star (MS star). This is a generally accepted overview of star formation.

1.2 Main stages of star formation

To delve deeper into the details of star formation requires a combination of accepted and disputed peer reviewed papers. This section will go deeper into star formation by discussing each of the main stages of star formation.

1.2.1 Giant molecular clouds and the Interstellar medium

The interstellar medium (ISM) is defined as the "stuff" that occupies the space between stars. This "stuff" is predominantly made up of matter and electromagnetic radiation. The ISM can be split up into five different thermal phases (Ryden & Pogge, 2016). The first phase is the hot ionized medium (HIM), this phase occupies ~50% of the volume inside the ISM. The HIM includes low density gas that is heated up to temperatures of over 10^6 K due to supernovas, powerful winds from the largest progenitor stars and UV radiation. The gas in the HIM can be detected by X-ray emission and absorption lines in the UV region of the spectrum.

The second phase is the warm ionized medium (WIM), Using results provided by Ferrière (2001), it is thought that this phase occupies ~15% of the volume inside the ISM and is made up of ionized hydrogen atoms (H^+ or HII). It is thought that most HII arises from the photoionization with strong UV radiation from O and B stars, which creates regions of HII around most O and B stars. The temperatures of the WIM range between 6000 to 10,000 K and is regulated by the heating of the photoionization of the hydrogen atoms and the cooling from Lyman alpha line emission (Lyα). The gas in the WIM can be traced using the Hα emission observed at a wavelength of 656.3nm.
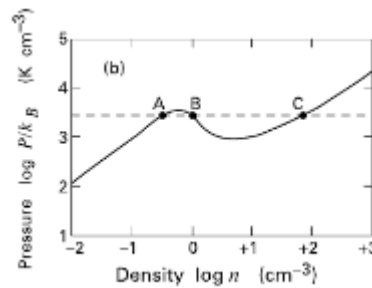

Figure 1 Theoretical prediction of equilibrium pressure as a function of number density. *(Wolfire, et al., 1995)*

The third and four phases are the warm neutral medium (WNM) and cold neutral medium (CNM); both phases together occupy ~34% of the volume inside the ISM and have number densities of $0.2 - 0.5$ and $50 - 100$ cm^{-3} for the WNM and CNM respectively, it is mostly made up of neutral hydrogen (HI) and is heated to ~8000 K in the WNM and $50 - 100$ K in the CNM. Both phases are heated by various ways, such as photoelectrons ejected from dust grains and cosmic rays ionizing atoms through collisions. It was first suggested by Field, et al. (1969) that the two phases are in thermal pressure equilibrium since $n_{WNM}T_{WNM} \approx n_{CNM}T_{CNM}$, where n is the density and T is the temperature. This agrees with the theoretical prediction for the equilibrium pressure as a function of density (as seen in Figure 1), where the WNM matches the stable point A and the CNM matches the stable point C, the point B represents an unstable point at which a perturbation causes the gas to fall into one of the stable points depending on the conditions of the perturbation. The CNM is cooled through the de-excitations of collisionally excited fine-structure lines of C^+ and other metals. The CNM can be traced using the C^+ emission line observed at a wavelength of 158μm (Bennett, et al., 1994). The WNM on the other hand has a very similar cooling mechanism to the WIM, where the Lyα emission is again the main cooling mechanism. The WNM can be traced using the 21cm emission line of HI formed due the spin-flip transition between two hyperfine energy levels, which was first discovered by Ewen & Purcell (1951).

The final phase is the molecular cloud, this phase is cold enough to give rise to interstellar molecular gas such as CN and CH (Swings & Rosenfeld, 1937), and were found through absorption lines produced in stellar spectra. The temperatures inside molecular clouds range between $\sim 10 - 20$ K with densities of over 10^3 cm^{-3} and occupies a volume of $< 1\%$ of the ISM. Although the molecular clouds only occupy

a very small percentage of the ISM, the contribution of the fractional ISM mass from molecular clouds is much greater than the volume of the ISM it occupies, due to the much heavier elements that are present in the molecular clouds compared to the other phases. The most abundant molecules in the molecular clouds are molecular hydrogen (H_2) and carbon monoxide (CO). Relative to the overall number of hydrogen nuclei, the abundance of H_2 is given by $x_{H_2} \approx 0.5$ and the abundance of CO is given by $x_{CO} \approx 1.4x10^{-4}$ (Clark, et al., 2012). Carbon monoxide arises in molecular clouds through a series of reactions between C^+, H_2 and neutral oxygen (OI). Although molecular hydrogen is the most abundant molecule in these molecular clouds, it is in fact the CO that is main cooling mechanism in the molecular clouds. It is suggested by Glover & Clark (2012) that H_2 provides a particularly inefficient cooling, due to widely spaced energy levels of ~ 170 J K, it is therefore particularly difficult to excite molecular hydrogen at low temperatures. The temperatures of the molecular cloud can reach as low as 10 K due to the rotational excitation of CO which has very low energy levels compared to that of hydrogen, and therefore can be exited at lower temperatures, resulting in cooling through the emitted photons that have been released from the rotational transition. The emission line of CO is the primary tracer of molecular clouds due to the high abundance of CO in molecular clouds. The C^+ fine structure excitation also plays a key role in cooling the molecular cloud and it was shown by Glover & Mac Low (2007) that C^+ could cool the molecular gas down to ~20 K. It was also suggested by Glover & Clark (2012) that molecular gas wasn't necessary due to C^+ cooling, however this is still heavily debated throughout the scientific community. It is often very difficult to observe molecular clouds due to the obscuration of starlight from interstellar dust as a result of absorption and scattering. Dust grains are solid materials composed mainly of carbon, silicon and oxygen and vary in size from a few microns down to the size of a few atoms (Draine, 2003). Dust provides another way of keeping the molecular clouds cool, through gas-grain collisions, the excited gas can release their energy to the dust grains in the form of collisions, which is then re-radiated away. When a molecular cloud contracts it behaves isothermally due to the mean free path of the photons realesed being very large and can be freely radiated away from the cloud (Ward-Thompson & Whitworth, 2011).

The largest of these molecular clouds are called Giant molecular clouds (GMC). Typically, they have masses greater than $\sim 10^4 \ M_\odot$ with similar properties to that of molecular clouds. It is generally agreed that most GMCs create filamentary structures through turbulence. Turbulence can be described as an unstable flow of gas and are still a highly-debated topic due to the very complicated physics involved. Usually the GMC will not have a uniform density throughout, instead most will have locally dense regions and tend to have dense cores. These cores are usually called 'starless cores' or 'pre-stellar cores' dependant on whether the core is gravitationally bound or not.
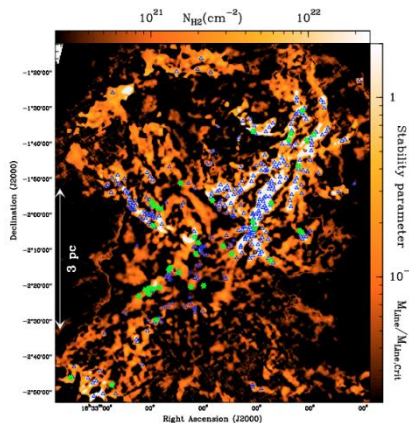
Figure 2 A column density map of Aquila derived from the SPIRE data. The candidate Class 0 protostars and bound prestellar cores identified in Aquila by *Bontemps, et al. (2010)* and *Könyves, et al. (2010)* are shown as green stars and blue triangles. *(André, et al., 2010)*
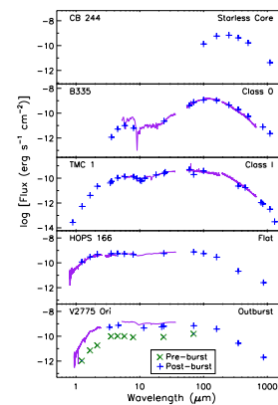
Figure 3 An example of SEDs for a starless core, a Class 0 protostar, a Class 1 protostar, a Flat-SED source and an outbursting Class 1 protostar. *(Dunham, et al., 2014)*

1.2.2 Filamentary structures and pre-stellar cores

Filamentary structures have been a renewed topic of interest thanks to the recent Gould Belt Survey, one of the key projects with *Herschel*. Filamentary structures are thin, elongated features with some of the highest colum densities observed in molecular clouds. Filaments were known long before *Herschel*, dating back to at least 1979 where Schneider & Elmegreen (1979) documented dark globular filaments. Arzoumanian, et al. (2013) suggest that filaments form through turbulences in the MCs, although further observations are needed to further our understanding of the formation of filaments. Evidence from *Herschel* suggests that prestellar cores result from the fragmentation of the filaments, and can be seen in Figure 2 (André, et al., 2010).

A pre-stellar core is defined as a dense core in a molecular cloud that is gravitationally bound and that will collapse into a star as they're self-gravitating. Pre-stellar cores are observed at far-infrared wavelengths, indicating that these cores are very cold (Ward-Thompson, et al., 2002). These pre-stellar cores can be characterized by looking at the spectral energy distribution (SED) as seen in Figure 3.

Stars form when pre-stellar cores become gravitationally unstable and begin to collapse, this occurs when gravity overcomes pressure, rotation, turbulence and magnetic fields. Assuming a spherical cloud of uniform density, a simple derivation can be made to find the distance at which the core collapses through equating the acceleration due to the pressure and the acceleration due to the gravitational force of the molecular cloud, this is called the Jeans length. This is stated as,

$$r_j \sim \frac{a_0}{(G\rho_0)^{\frac{1}{2}}} \tag{1}$$

where r_0 is called the Jeans length, a_0 is the isothermal sound speed, G is the gravitational constant and ρ_0 is the initial uniform density (Ward-Thompson & Whitworth, 2011). We can also find the minimum mass associated with the Jeans length, which is stated as,

$$M_j \sim \frac{4\pi a_0^3}{3(G^3\rho_0)^{\frac{1}{2}}} \tag{2}$$

where M_j is the Jeans mass. This is the minimum mass at which the core starts to collapse due to its own self-gravity. Therefore, the mass of the cloud must be greater than the Jeans mass in order for the core to collapse. We state a dependency of the Jeans mass with the temperature of the cloud through equating the internal energy of the cloud and its kinetic energy,

$$M_j \propto T^{\frac{3}{2}} \tag{3}$$

where T is the temperature of the cloud. Therefore, if the temperature was to increase the Jeans mass would also increase. To understand the duration of the core collapse, we can derive a timescale using crude assumptions, such as a pressure-free collapse,

$$t_{ff} = \left(\frac{3\pi}{32G\rho}\right)^{\frac{1}{2}} \tag{4}$$

where t_{ff} is the free-fall timescale. The collapse of a core is roughly an order of magnitude larger than the free-fall timescale due to the influence of the magnetic field and turbulences, which suggests that the cores are not in free-fall collapse (Ward-Thompson & Whitworth, 2011; Ward-Thompson & Jessop, 1996).

1.2.3 Fragmentation and Protostars

It was previously thought that parts of the cloud break up into smaller fragments during a collapse through hierarchical fragmentation, since the density of the cloud increases during the contraction, the Jeans mass decreases and parts of the original cloud become gravitationally unstable and start to contract on themselves leading to fragmentation. This process was thought to be based on a homologous collapse (Hunter, 1964), but due to the recent survey, it is now proposed that filaments fragment into prestellar cores when areas of the filaments surpass the Jeans mass, these cores then undergo further fragmentation (André, et al., 2010). During the collapse phase of a prestellar core, the prestellar core is thought to fragment into smaller cores which collapse and form groups of protostars (André, et al., 2009). The opacity of a protostar eventually is at a point where photons can no longer be freely radiated away, which causes an increase in its temperature. The Jeans mass increases due to equation 3, which leads to the protostar to be gravitationally stable. Roughly two-thirds all protostars form binary and multiple systems (Ward-Thompson & Whitworth, 2011). These multiple star systems tend to form very elliptical orbits and the eccentricity of the orbit can yield the shape of the orbital path of ,which is stated as,

$$e = \frac{r_a - r_p}{r_a + r_p} \tag{5}$$

where e is the eccentricity of the orbit, r_a is the apocenter, r_p is the pericenter.

These protostars are buried deep inside a gaseous envelope with a surrounding circumstellform binary and ar disk that is produced due to the angular momentum of the protostar, and can only be observed through outflow presence. At this stage in time protostars can be classified as Class 0 objects that can be inferred via the SED as seen in Figure 3 (Andre, et al., 1993; Dunham, et al., 2014). The protostar remains cool due to the low opacity, and the photons keep freely radiating away from the protostar. The collapse also maintains its low temperature due to cooling from colliding dust grains. The surrounding envelope accretes onto the protostar through Bondi-Hoyle accretion. Assuming a spherically symmetric accretion, Bondi-Hoyle accretion is where the protostar accretes matter through gravity and traces a cylinder through the envelope due to the differences in the relative motion of the envelope and the protostar and accretes matter as its moving through the envelope (Bondi, 1952). The protostar can be classed as a Class I object at this point and can be inferred via the SED as seen in Figure 3. The protostar is said to be a Class II object once the surrounded envelope has been accreted onto the protostar. It is thought that most of the circumstellar disks accretes onto the protostar and leads to the formation of remnant disks, at this point the protostar is said to be a pre-main-sequence stars (PMS star) and can also be classed as a Class III object.

The initial mass function (IMF) can be used to find the probable number of stars formed in a given molecular cloud with mass, M, and is usually represented as a probability distribution function. This was first derived by Salpeter (1955) who suggested that the IMF follow's a power-law distribution and has since been improved upon by Kroupa (2001). The IMF can be stated as,

$$\xi = \xi_0 M^{-\alpha} \tag{6}$$

where ξ is the star formation rate, M is the total mass of stars formed and α varies 2.35 for $M > 0.5 M_\odot$, 1.3 for $0.08 M_\odot < M < 1 M_\odot$ and 0.3 for $M < 0.08 M_\odot$.

2. Outline

Due to the recent findings of the Gould Belt Survey, filamentary structures have received recent special interest and have now surpassed the older theories of a spherical collapse. Our project intends to rectify some of the research made on protostars that assumed spherical collapse, through researching protostars inside filamentary structures. Our goal is to create initial conditions that represent our current understanding of how protostars behave inside these filamentary structures by modelling a N-body

simulation of these protostars inside filaments. One of many possible outcome from our simulation could lead to ejecta's of protostars from these filaments, formation of binary stars and the eccentricity of protostellar orbits, our project will try to achieve these possible results from our initial conditions. To model the orbital path of the protostars, we use a modified version of Newtons law of Gravity which was originally formalized by Sverre Aarseth, who created the NBODY codes. We use the NBODY2 code which states that,

$$\ddot{r}_i = -G \sum_{j=1; j \neq i}^{N} \frac{m_j(r_i - r_j)}{(r_{ij}^2 + \epsilon^2)^{3/2}} \tag{7}$$

where $\ddot{r}$ is the gravitational acceleration on a protostar of index i, G is the gravitational constant, the j notation is for all the other particles with mass m_j and coordinates r_j and finally the softening parameter is defined as ϵ. The introduction of a softening parameter prevents a singularity as the separation of r_{ij} tends to zero (Aarseth, 2001). Using the acceleration of the particles, the orbits can be found through numerical integration using a computer programming language, usually C, C++ or Fortran. The Verlet method was the most suitable method of integration for us due to its simplicity and its higher order accuracy over the Euler method, which can be stated as,

$$r(t + \Delta t) = r(t) + v(t)\Delta t + \frac{1}{2}\ddot{r}(t)\Delta t \tag{8}$$

$$v(t + \Delta t) = v(t) + \frac{1}{2}\big(\ddot{r}(t) + \ddot{r}(t + \Delta t)\big)\Delta t \tag{9}$$

where $\ddot{r}(t)$, $v(t)$, $r(t)$ and Δt are the acceleration, velocity, coordinate and the time-step of a protostar at time t respectively (Swope, et al., 1982). Adaptive time-steps are a way of keeping the workload down whilst improving the accuracy of our numerical integration. In our project, we use an adaptive time-step used in the GADGET-2 code (Springel, 2005), which is defined as,

$$\Delta t_{grav} = min\left[\Delta t_{max}, \left(\frac{2\eta\epsilon}{|\ddot{r}|}\right)^{\frac{1}{2}}\right] \tag{10}$$

where Δt_{grav} is the adaptive time-step, Δt_{max} is the maximum time-step that we define and η is an accuracy parameter.

3. Preliminary results

We use a Sun-Earth-Moon model to verify a working code due to the orbits of the model being well known. To test the adaptive time-steps of our code, we decided to model a very eccentric orbit due to the varying acceleration of the eccentric orbit. The orbits of both models can be seen below.
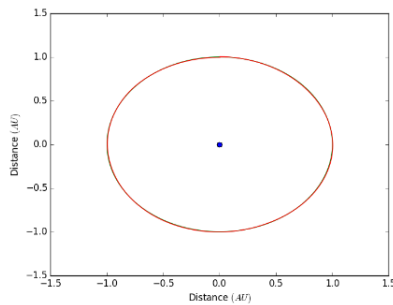
Figure 4 A graph of the orbital paths of Earth (green) and the moon (red) with the sun at the centre (blue).
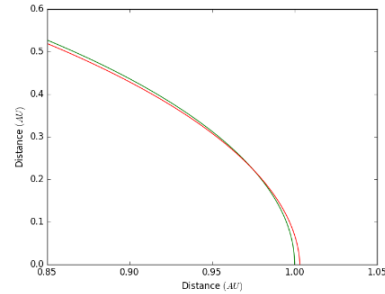
Figure 5 A close up on the orbital paths of Earth (green) and the Moon (red) to see the interaction between the two bodies.

The behaviour of the orbital paths of the Sun-Earth-Moon model is consistent with the well-known observations of the solar system. From Figure 4, we can see both the Earth and the Moon orbit around the Sun, and Figure 5 shows that the Moon also orbits the Earth, which agrees with observations.

To test the adaptive time-step in our code, we used an eccentric orbit that varies considerably with acceleration, which should in turn vary the time-step using equation 10.
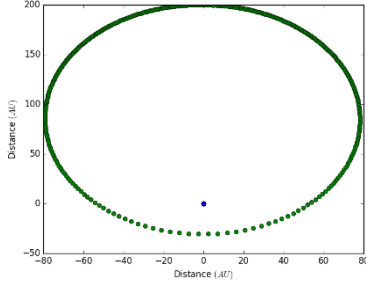
Figure 6 A graph showing the positions of the eccentric orbit of the body at each time-step using a constant time-step
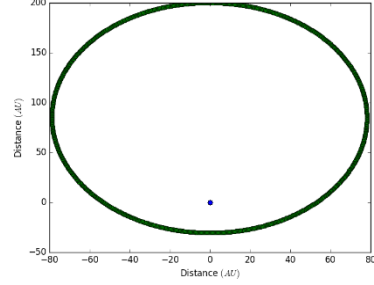
Figure 7 A graph showing the positions of the eccentric orbit of the body at each time-step using an adaptive time-step

To verify that the adaptive time-step works, we decided to compare the adaptive time-step with a constant time-step, which can be seen in Figures 6 and 7. It is clear that the points at the perihelion of the adaptive time-steps (see Figure 7) are more closely spaced in comparison to the constant time-steps (see Figure 6), suggesting that the we have a working adaptive time-step code.

4. Discussion and conclusions

To further our project, we will define and apply our initial conditions to our N-body code, which consists of a cylinder like structure for the filament with dimensions of 0.1 parsec for the radius and 1 parsec for the length. Multiple groups of protostars with sizes of around 200 AU will be spaced at around 600 to 20,000 AU apart from one another, which arise due to the fragmentation of the filament. Within these groups, protostars will be randomly positioned with masses chosen from the IMF. The velocities of these protostars will be chosen at random but will be scaled so that the groups of protostars remain initially gravitationally bound. Using our initial conditions, we shall record the interactions between each protostar and also between the groups, along with any ejecta and close encounters. Using the results gathered we can then compare with future surveys such as Gaia-ESO Survey which is currently ongoing.

C1331824

References

Aarseth, S. J., 2001. NBODY2: A direct N-body integration code. *New Astronomy,* Volume 6, pp. 277-291.

André, P., Basu, S. & Inutsuka, S., 2009. The formation and evolution of prestellar cores. *Cambridge University Press,* p. 254.

André, P. et al., 2010. From filamentary clouds to prestellar cores to the stellar IMF: Initial highlights from the Herschel Gould Belt Survey. *Astronomy and Astrophysics,* Volume 518, p. L102.

Andre, P., Ward-Thompson, D. & Barsony, M., 1993. Submillimeter continuum observations of Rho Ophiuchi A - The candidate protostar VLA 1623 and prestellar clumps. *Astrophysical Journal,* Volume 406, pp. 122-141.

Appenzeller, I., Lequeux, J. & Silk, J., 1980. *Star Formation.* 10th ed. : Swiss Society of Astronomy and Astrophysics.

Arzoumanian, D., André, P., Peretto, N. & Könyves, V., 2013. Formation and evolution of interstellar filaments. Hints from velocity dispersion measurements. *Astronomy & Astrophysics,* Volume 553, p. A119.

Bennett, C. et al., 1994. Morphology of the interstellar cooling lines detected by COBE. *Astrophysical Journal,* Volume 434, pp. 587-598.

Bondi, H., 1952. On spherically symmetrical accretion. *Monthly Notices of the Royal Astronomical Society,* Volume 112, p. 195.

Bontemps, S. et al., 2010. The Herschel first look at protostars in the Aquila rift. *Astronomy and Astrophysics,* Volume 518, p. L85.

Clark, P., Glover, S., Klessen, R. & Bonnell, I., 2012. How long does it take to form a molecular cloud. *Monthly Notices of the Royal Astronomical Society,* Volume 424, pp. 2599-2613.

Draine, B. T., 2003. Interstellar Dust Grains. *Annual Review of Astronomy &Astrophysics,* Volume 41, pp. 241-289.

Dunham, M. M. et al., 2014. The Evolution of Protostars: Insights from Ten Years of Infrared Surveys with Spitzer and Herschel. *Protostars and Planets VI,* Volume 914, pp. 195-218.

Ewen, H. I. & Purcell, E. M., 1951. Observation of a Line in the Galactic Radio Spectrum: Radiation from Galactic Hydrogen at 1,420 Mc./sec.. *Nature,* Volume 168, p. 356.

Ferrière, K., 2001. The interstellar environment of our galaxy. *Reviews of Modern Physics,* Volume 73, pp. 1031-1066.

Field, G. B., Goldsmith, D. W. & Habing, H. J., 1969. Cosmic-Ray Heating of the Interstellar Gas. *Astrophysical Journal,* Volume 155, p. 149.

Glover, S. & Clark, P., 2012. Is molecular gas necessary for star formation?. *Monthly Notices of the Royal Astronomical Society,* Volume 421, pp. 9-19.

Glover, S. O. & Mac Low, M.-M., 2007. Simulating the Formation of Molecular Clouds. II. Rapid Formation from Turbulent Initial Conditions. *The Astrophysical Journal,* Volume 659, pp. 1317-1337.

Hunter, C., 1964. The Development of Gravitational Instability in a Self-Gravitating Gas Cloud. *Astrophysical Journal,* Volume 139, p. 570.

Könyves, V. et al., 2010. The Aquila prestellar core population revealed by Herschel. *Astronomy and Astrophysics,* Volume 518, p. L106.

Kroupa, P., 2001. On the variation of the initial mass function. *Monthly Notices of the Royal Astronomical Society,* Volume 322, pp. 231-246.

Ryden, B. & Pogge, R., 2016. *Interstellar and Intergalactic Medium.* 2nd ed. : The Ohio State University.

Salpeter, E. E., 1955. The Luminosity Function and Stellar Evolution. *Astrophysical Journal,* Volume 121, p. 161.

Schneider, S. & Elmegreen, B. G., 1979. A catalog of dark globular filaments. *Astrophysical Journal Supplement Series,* Volume 41, pp. 87-95.

Springel, V., 2005. The cosmological simulation code GADGET-2. *Monthly Notices of the Royal Astronomical Society,* Volume 364, pp. 1105-1134.

Stahler, S. & Palla, F., 2008. *The formation of stars.* : Wiley-VCH.

Swings, P. & Rosenfeld, L., 1937. Considerations Regarding Interstellar Molecules. *Astrophysical Journal,* Volume 86, pp. 483-486.

Swope, W. C., Andersen, H. C., Berens, P. H. & Wilson, K. R., 1982. A computer simulation method for the calculation of equilibrium constants for the formation of physical clusters of molecules: Application to small water clusters. *The Journal of Chemical Physics ,* Volume 76, p. 637.

Ward-Thompson, D., André, P. & Kirk, J. M., 2002. The initial conditions of isolated star formation - V. ISOPHOT imaging and the temperature and energy balance of pre-stellar cores. *Monthly Notices of the Royal Astronomical Society,* Volume 329, pp. 257-276.

Ward-Thompson, D. & Jessop, N. E., 1996. The Initial Conditions of Star Formation: A Study of Pre-Stellar Cores. *Newsletter on Analysis of Astronomical Spectra,* p. 19.

Ward-Thompson, D. & Whitworth, A., 2011. *An Introduction to Star Formation.* : Cambridge University Press.

Wolfire, M. et al., 1995. The neutral atomic phases of the interstellar medium. *Astrophysical Journal,* Volume 443, pp. 152-168.

Appendix

The code used to find the orbital paths can be seen below.

```python
#!/usr/bin/env python
"""
Created on Tue Oct 18 09:11:38 2016

@author: C1331824
"""

from __future__ import division
import numpy as np
import scipy.constants as sc
from numpy import linalg as LA

from Verlet_IC_EMS import *

####################

def Verp(ovel, opos, dt, a):
    "Position:"
    pos = opos + ovel*dt + .5*a*dt**2
    return pos

def Verv(pos, mass, ovel, dt, a, e):
    "Velocities:"
    an, pe = acc(pos, mass, ovel, e)
    vel = ovel + .5*(a + an)*dt
    return vel

def acc(pos, mass, vel, e):

    a = np.zeros((N,3))
    pe = np.zeros((N,1))

    G = sc.gravitational_constant

    for i in range(0,N-1):
        for j in range(i+1,N):

            r = pos[i]-pos[j]
            m = LA.norm(r)
            F = (G/(m+e)**3)*r

            # acceleration
            a[i] += -F*mass[j]
            a[j] += F*mass[i]
            # potential energy
            pe[i] += -(G*mass[i]*mass[j])/(m+e)
            pe[j] += -(G*mass[j]*mass[i])/(m+e)

    return a, pe

def KE(vel, mass):
    # kinetic energy
    ke = np.zeros((N,1))

    for i in range(0,N):
        vi = LA.norm(vel[i])
        ke[i] = .5*mass[i]*vi**2

    return ke

while t < t_max:

    ac, pe = acc(pos, mass, vel, e)

    ke = KE(vel,mass)

    dt_grav =  np.min([dt_max,((2*n*e)/(np.max(LA.norm(ac, axis = 1))))**.5])

    print(t/t_max)*100

    "Verlet Method"
    opos = pos
    ovel = vel

    pos = Verp(ovel, opos, dt_grav, ac)
    vel = Verv(pos, mass, ovel, dt_grav, ac, e)

    t += dt_grav

    if t == t_max:
        break
```